Holographic storage of ultrafast photonic qubit in molecules

Alexis Voisine, Franck Billard, Olivier Faucher, Pierre Béjot, Edouard Hertz

Abstract We demonstrate that ultrashort spatially structured beams can sculpt a sample of gas-phase molecules like a 4D material so as to produce a spatial pattern of aligned molecules whose shape and temporal evolution allow to restore the spatial light information on a time-delayed reading pulse. To do so, the spatial phase and amplitude information of ultrashort light beams is encoded into rotational coherences of molecules by exploiting the interplay between spin angular momentum and orbital angular momentum. The field-free molecular alignment resulting from the interaction leads to an inhomogeneous spatial structuring of the sample allowing to transfer the encoded information into a time-delayed probe beam. The demonstration is conducted in CO_2 molecules. Besides applications in terms of THz bandwidth buffer memory, the strategy features interesting prospects for establishing versatile optical processing of OAM fields, for studying various molecular process or for designing new photonic devices enabling to impart superpositions of OAM modes to light beams.

Holographic storage of ultrafast photonic qubit in molecules

Alexis Voisine, Franck Billard, Olivier Faucher, Pierre Béjot and Edouard Hertz*

1. Introduction

The ability to establish fine control of matter with light or, conversely, manipulating light on demand with matter has opened up fascinating applications ranging from coherent and quantum control, [1,2] to laser structuring process, [3] via pulse shaping technologies, [4] laser filamentation, [5] fiber communication [6] or data storage [7] to name a few. In this context, there has been a growing interest over the past few decades in the use of spatially structured optical waveforms, especially those embedding orbital angular momentum (OAM). [8–11] Such fields are characterized by a helical phase distribution $\ell\varphi$, where φ is the azimuthal angle in the transverse plane of the beam, and where ℓ, the topological charge, corresponds to the number of interwined helical phase over one propagation wavelength. [8] Light-matter interaction with such fields have been extensively investigated. The matter can be used as an interface to store [12–14] or manipulate [15] structured light beams, while interaction of OAM beams with matter has found far-reaching applications covering innovative photonic functionalities, [16] particle manipulation, [17,18] quantum information technology, [19–21] optical communication, [22–25] laser micromachining [26] or high-resolution imaging, [27] to cite only a few. The interweaving between chirality of light and matter [28–30] as well as the interaction of matter with multiplexed light embedding both spin angular momentum (SAM) and OAM, [31,32] constitute new emerging paradigm of great importance. In this frame, we have recently reported [33] the use of gas-phase molecules as a quantum interface to store pure OAM states carried by ultrashort laser pulses. Through a coupling scheme exploiting the interplay between SAM and OAM, the helical phase information of light beams was encoded into the rotational coherences of linear molecules. The underlying mechanism at the origin of this storage was explained by the spatial structuring of the molecular sample induced by the field. The polarization vector distribution of the writing field was shown to induce an inhomogeneous spatial distribution of molecular axes orientation in the transverse plane of the beam. This last was found to follow the same azimuthal pattern as the one of neutral axes of q-plates, [15] commonly used for the production of OAM beams. The periodical revival of this "molecular q-plate" associated with the quantum beatings of the rotational wavepacket was exploited to restore the encoded helical phase structure on-demand. Although the strategy has proven its suitability for memorizing a spatial phase pattern, the ability of the method to store a spatial amplitude information, in addition to a spatially varying phase, remains to be demonstrated. Such a property turns out to be particularly relevant for encoding a coherent superposition of different OAM, namely an OAM-based photonic qubit, carried by an ultrashort laser pulse. A coherent superposition of OAM bears both spatial phase and amplitude modulation requiring, for its storage, more elaborate molecular structuring than that required with a pure OAM. While for pure OAM, the molecules have to be confined into the transverse plane of the beam along a specific direction depending on the azimuthal angle, the storage mechanism of the present work can be interpreted by the production of a spatial pattern of aligned molecules in 3 dimensions (which evolves over time). This specific and refined structuring allows to restore the overall information on a time-delayed reading pulse. The experiment is conducted in CO_2 molecules at room temperature with the storage of a superposition of $\ell = \pm 1$ OAM states, also called photonic gear. The choice of this molecule was driven by its large polarizability anisotropy but the method is applicable to all molecules except spherical top molecules. The restored state is analyzed for different relative amplitude or phase between the two components and our observations reveal a great fidelity in the preservation of the mode superposition validating the ability of the storage process. The experimental observations are supported by a theoretical model to capture the underlying effects.

Laboratoire Interdisciplinaire Carnot de Bourgogne, UMR 6303 CNRS - Université Bourgogne Franche-Comté, 21078 Dijon Cedex, France
* Corresponding author: e-mail: edouard.hertz@u-bourgogne.fr

2. Principle

The photon state of the input field to be stored (called "input beam" hereafter) can be written as:

$$|\Psi\rangle_{\text{in}} = a_1 |+1\rangle + a_{-1} e^{i\beta} |-1\rangle \qquad (1)$$

with $a_1^2 + a_{-1}^2 = 1$ (a_1 and a_{-1} being real and positive) and $|\ell\rangle$ the OAM mode of topological charge ℓ. This state corresponds to a coherent superposition of two OAM modes with a phase shift β. In practice, the storage in atomic states of such structured light beams is obtained using an auxiliary beam, ideally a plane wave, analogously to holography imaging. Excitation schemes are usually based on a resonant Λ-configuration, with the absorption (resp. emission) of one photon of the structured beam (resp. auxiliary beam) in the stimulated Raman process. The spatial phase and amplitude information, stored through the coherences induced between the two lower states, can be restored at will with a reading beam. Such a strategy has been successfully applied to the storage of spatial information embedded into narrowband laser beams [13,14] in resonance with an excited state. The coupling scheme of the present work relies for its part on a non-resonant Λ excitation scheme (see Fig. 1) well-suited for the storage of spatial information carried by broadband laser pulses. We point out that this configuration is standard for the production of rotational coherences and field-free molecular alignment in molecular systems. [34] As depicted in Fig. 1, an ultrashort pump

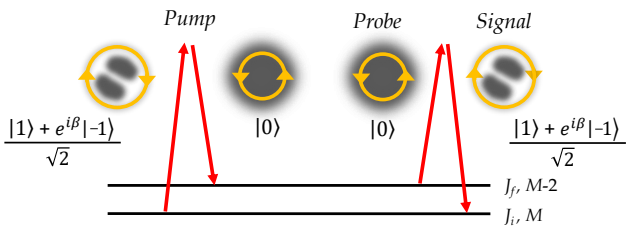

Figure 1 Coupling scheme for encoding structured fields embedding OAM modes into rotational states of molecules. The SAM conservation allows transitions $\Delta J = J_f - J_i = 0, \pm 2$, $\Delta M = +2$ ($\Delta M = -2$) for the probe (pump) interaction.

pulse consisting of the field carrying the OAM superposition $|\Psi\rangle_{\text{in}}$ and the auxiliary field ($|\ell = 0\rangle$) interact with the molecular sample. This interaction stores the spatial information (phase and amplitude) of the input beam by producing a rotational wavepacket in the vibronic ground state of the molecules. The encoded spatial structure can be restored later on with a time-delayed probe pulse by exploiting the quantum beating of the wavepacket. We recall that with short pulses (of duration much shorter than the rotational period of the molecules), the interaction prepares a broad rotational wavepacket in the ground state of the molecule by impulsive stimulated Raman transitions. The periodical rephasing of the rotational wavepacket then manifests itself by the occurrence of molecular alignment [34] at well-defined times after the pulse turn off. The induced anisotropy is exploited for the restoration of the spatial information. As explained in Ref. [33] the sequence of photons implied in the Raman process for such a non-resonant and broadband excitation is not well determined when using linear polarizations. Besides the sequence of photons depicted in Fig. 1, the pump excitation can also be achieved with either one of the two beams alone (input or auxiliary), or by exchanging the input and auxiliary beam. This results in the occurrence of unwanted quantum excitation channels detrimental to the information to be encoded: the channel only driven by the auxiliary beam stores $|0\rangle$ while the one by the structured field a superposition of $|0\rangle$, $|2\rangle$, and $|-2\rangle$. The relevant information to be stored can nevertheless be preserved from this uncontrolled superposition by using circular polarizations of opposite helicity for the two fields implied in the Raman transition as depicted in Fig. 1. Such a strategy enables the selection of one specific quantum channel by spin constraint. In our experiment, the SAM and OAM are conserved on their own since the weak focusing geometry prevents any spin-to-orbital conversion [35] and since dipole electric transition are allowed with no significant role played by quadrupole transitions. [36] In the scheme of Fig. 1, a left circularly polarized (LCP) probe field is used to read the medium at the occurrence of field-free molecular alignment producing a field of opposite helicity, i.e. right circularly polarized (RCP), due to the sample anisotropy. This "signal" field is isolated by a circular analyzer in our experiment. Using the convention from the point of view of the receiver for the SAM, the corresponding Raman coupling of the reading process implies $\Delta J = 0, \pm 2$ and $\Delta M = +2$ transitions, where J and M correspond to the total angular momentum and magnetic quantum numbers respectively. The sequence of pump pulses helicity in the global parametric process is then constrained by SAM conservation imposing a sequence of RCP-LCP for the pump Raman excitation as depicted in Fig. 1. Depending on their polarization, the spin constraint therefore assign the role played by both input and auxiliary beams in the excitation, preventing unwanted quantum channels. This strategy has been successfully applied to the storage of pure OAM modes [33] embedding spatial phase modulation and the purpose of the present work is to study a possible operation with OAM's superpositions bearing both spatial phase and amplitude structures.

3. Theoretical model

In order to assess the ability of the method to operate with fields carrying an OAM superposition state, we write the time-dependent Hamiltonian interaction describing the coupling of the molecule with the pump field. This last (propagating along $\mathbf{z}$) is written in circular basis as $\mathbf{E} = E_{\text{L}}\mathbf{e}_{\text{L}} + E_{\text{R}}\mathbf{e}_{\text{R}}$, where $\mathbf{e}_{\text{R}}$ (resp. $\mathbf{e}_{\text{L}}$) corresponds to the right (resp. left)-handed circular polarization in the (x,y) plane, namely $\mathbf{e}_{\text{R}} = \frac{1}{\sqrt{2}}(1,-i)$ and $\mathbf{e}_{\text{L}} = \frac{1}{\sqrt{2}}(1,i)$. According to the excitation scheme of Fig. 1, E_{L} corresponds to the auxiliary field while E_{R} is the phase and amplitude structured light

beam to be stored that can be written as:

$$E_{\mathrm{R}}(t,\varphi) = \varepsilon_0(t)a_s(\varphi)e^{-i[\omega_0 t-\phi_s(\varphi)]} \quad (2)$$

$$E_{\mathrm{L}}(t) = \varepsilon_0(t)e^{-i\omega_0 t}, \quad (3)$$

where $\varepsilon_0(t)$ and ω_0 denote the pulse envelope and the central angular frequency of the pulse. $a_s(\varphi)$ and $\phi_s(\varphi)$ stand for the spatial amplitude and phase of the beam to be encoded that are related to the parameters a_1, a_{-1}, and β of Eq. 1 [See section 2, Supporting Information]. The spatial amplitude $a_s(\varphi)$ (real and positive) includes a possible global amplitude factor between the components E_{R} and E_{L}. We point out that, for sake of clarity, the radial dependance has been omitted in these expressions since the relevant information in our case is encoded into the azimuthal coordinate φ (a radial dependance would not change the main conclusion). Within the high-frequency approximation, one can show [See section 3, Supporting Information] that the Hamiltonian interaction can be written as:

$$\begin{aligned} H_{\mathrm{int}} = &-\frac{1}{8}\varepsilon_0(t)^2(a_s(\varphi)-1)^2\Delta\alpha\sin^2\theta \\ &-\frac{1}{4}\varepsilon_0(t)^2(a_s(\varphi)^2+1)\alpha_\perp \\ &-\frac{1}{2}\varepsilon_0(t)^2 a_s(\varphi)\Delta\alpha\sin^2\theta\cos^2\left(\Phi-\frac{\phi_s(\varphi)}{2}\right), \end{aligned} \quad (4)$$

where θ and Φ are the Euler angles of the molecule with θ the angle between the molecular axis and the fixed-frame quantum axis $\vec{z}$ (corresponding to the propagation axis for all fields) and Φ the azimuthal angle (with respect to the fixed-frame $\vec{x}$-axis) of the projection of the molecular axis onto the $x-y$ plane. $\Delta\alpha = \alpha_\parallel - \alpha_\perp$ is the difference between the parallel and perpendicular components of the polarizability tensor. The first two terms of the Hamiltonian, independent of Φ, are associated to transitions $\Delta M = 0$ and correspond to the excitation channels only driven by the input field or the auxiliary field as explained before. It can be noted that these two terms do not induce any preferential direction of the molecules in the transverse plane and therefore do not contribute to produce any anisotropy for the reading beam. Only the last term of the interaction Hamiltonian relies on the $\Delta M = \pm 2$ transitions of interest here that contribute to the measured signal in the experiment (see Fig. 1). This last term tends to preferentially confine the molecules in the (x,y) plane (corresponding to $\theta = \pi/2$) at an angle $\Phi = \frac{\phi_s(\varphi)}{2}$ that depends on the azimuthal coordinate φ inside the beam. This coupling term varies linearly with $a_s(\varphi)$ the spatial amplitude of the input field so that the induced alignment (in the transverse plane) is expected to follow the same trend at least below the saturation regime. [37] The direction and amplitude of molecular alignment therefore depends on the coordinate φ of the molecule inside the beam. A probe beam $E_{\mathrm{pr}}(t)$ interacting with such a structured medium will experience a spatially-dependent modification of its ellipticity at the origin of the OAM superposition carried by the signal field, namely the field of opposite helicity isolated by the circular analyzer (Fig. 1). By calculating the dipole moment resulting from the interaction of the probe pulse with the molecular sample [See section 3, Supporting Information], the signal field writes as:

$$E_{\mathrm{sig}}(t,\varphi) \propto \Delta\alpha \left\langle \sin^2\theta e^{i2\Phi} \right\rangle (t,\varphi) E_{\mathrm{pr}}(t). \quad (5)$$

We consider a probe pulse time-delayed by τ of the form $E_{\mathrm{pr}}(t) = \varepsilon_0(t-\tau)e^{-i\omega_0(t-\tau)}$. For a molecular alignment along $\theta \approx \pi/2$ and $\Phi \approx \frac{\phi_s(\varphi)}{2}$, varying with the amplitude $a_s(\varphi)$ as discussed above, the signal field becomes:

$$\begin{aligned} E_{\mathrm{sig}}(t,\varphi) &\propto \varepsilon_0(t-\tau)a_s(\varphi)e^{-i(\omega_0(t-\tau)-\phi_s(\varphi))} \\ &\propto E_{\mathrm{R}}(t-\tau,\varphi), \end{aligned} \quad (6)$$

which is a replica of the RCP pump field encoded into the molecular sample with the same amplitude and phase distribution. It should therefore be possible to store and restore any OAM or superposition of OAM in this way.

4. Experimental set-up & results

The experimental set-up to verify this prediction is shown in Fig. 2. Briefly, the laser system produces pulses of 35 fs duration centered around 800 nm at 1 kHz repetition rate and of maximum energy 5 mJ. The beam is split into three parts so as to produce the input and auxiliary components of the pump beam as well as the probe beam. The production of the pump beam is depicted in Fig. 2(b). The OAM superposition is produced with a q-plate [15] enabling to generate OAM beams via SAM-OAM exchange. The chosen q-plate (half-waveplate, q=1/2) in conjunction with a Berek compensator (BC_3) and a polarizer encodes the superposition of OAM modes $|\Psi\rangle_{\mathrm{in}}$ of Eq. 1 at once into the beam [See section 1, Supporting Information]. This structured beam is then recombined with a part of the incident beam, the auxiliary beam $|0\rangle$ ["Aux" in Fig. 2(b)], passing through a delay line and whose polarization is rotated by 90° with a half waveplate. Both components, temporally synchronized, are recombined with a beam splitter (BS), and circularly polarized with an opposite handedness by a quarter waveplate so as to produce the overall pump field. The probe beam for its part is frequency doubled with a BBO-crystal, circularly polarized and time-delayed with a delay-line [Fig. 2(a)]. Pump and probe beams, recombined by an optical wedge, propagate along the same axis and are focused by a lens (f=30 cm) in a static cell filled with 1 bar of CO_2. At the exit of the cell, the probe is filtered from the pump with a dichroïc filter. A circular analyzer (BC_2 with polarizer) isolates the signal field produced during the interaction which can be measured either by a CCD camera to get its spatial profile, or by a photomultiplier (PM), for having the spatially-integrated signal. The spatial phase profile is obtained by measuring the interference pattern with a reference plane wave [called "Ref" in Fig. 2(a)] of same polarization state.

The first experiments have been conducted with a superposition of balanced $|\pm 1\rangle$ OAM states, namely $|\Psi\rangle_{\mathrm{in}} =$

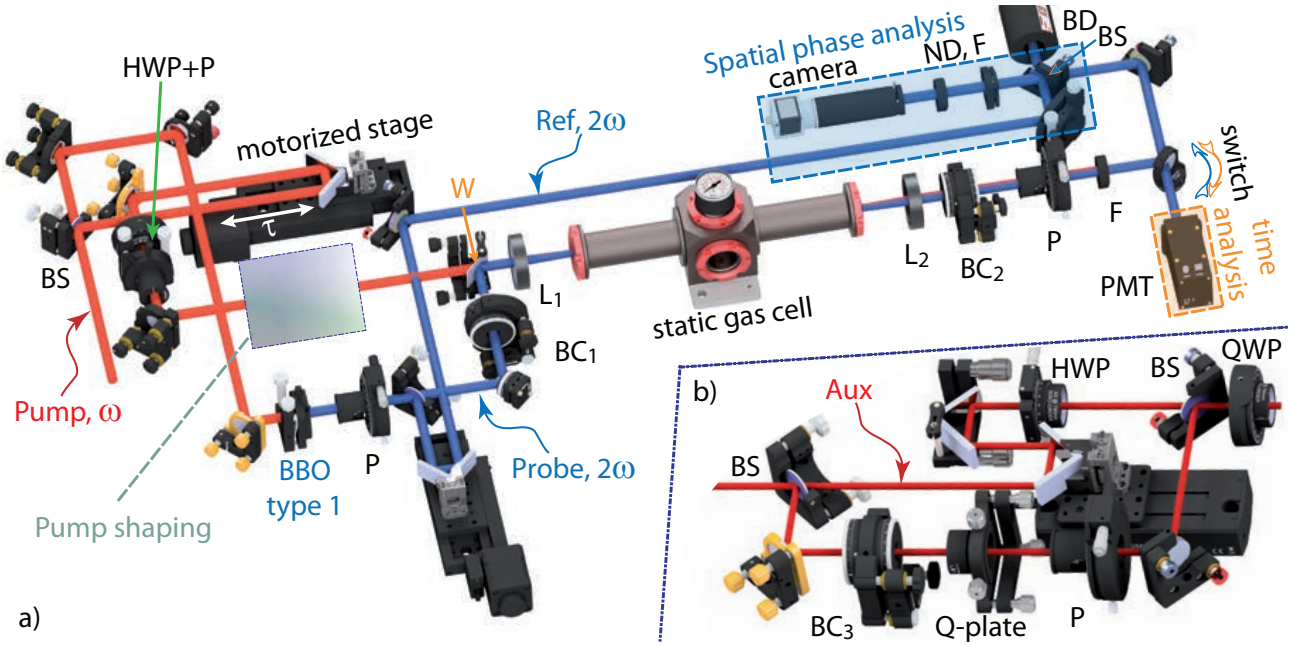

Figure 2 (a) Overview of the experimental set-up. BS: beam splitter, W: wedge, BBO: type 1 doubling crystal, P: Polarizer, L: plano-convex lens, BC: Berek compensator, PMT: photomultiplier tube, BD: beam dump, F : 400 nm bandpass filter, ND: neutral density filter. (b) Production of the pump beam (input and auxiliary): Q-plate: q-plate [half-waveplate, $q = 1/2$], HWP: half waveplate, QWP: quarter waveplate

$\frac{|1\rangle+e^{i\beta}|-1\rangle}{\sqrt{2}}$ in Eq. 1. It corresponds to a field amplitude varying as $\cos(\varphi-\beta/2)$, where the dephasing β can easily be tuned by modifying the neutral axis orientation of the Berek compensator before the q-plate [See section 1, Supporting Information]. Typical results are depicted in Fig. 3 where all signals (shown in left column) have been measured at a pump-probe delay of $\tau = 21.18$ ps. Such a delay corresponds to a revival peaks of molecular alignment but similar results can be obtained at any other delays and even between two revivals as already discussed. [33] The first line [Fig. 3(a,d)] corresponds to the case $\beta \approx 0$. The spatial distribution of the restored signal field, displayed in Fig. 3(a), shows a petal-like pattern which is characteristic of a superposition of two conjugate ($\pm\ell$) OAM modes. The number of petals and their orientation is in perfect agreement with the expectation 2ℓ petals around $\varphi = 0,\ \pi$. It reproduces with a good fidelity the spatial distribution of the input beam encoded into the molecular sample and shown in inset of the right panel. Besides the intensity distribution, another important ingredient of the restoration is the spatial phase, experimentally characterized from the interference pattern with a reference beam. This last, displayed as a color scale in Fig. 3(a), well reproduces the expected π-phase shift between the two lobes of the field pattern. We also proceeded to the decomposition of the signal field into the first OAM eigenstates. As observed in Fig. 3(d), the dominant contributions are concentrated within the $\ell = \pm 1$ modes of similar amplitude in agreement with the spatial shaping of the field applied by the combination of the Berek compensator (tuned as a half-waveplate) and the q-plate ([See section 1, Supporting Information]. Others configurations with different relative phases β [$\beta \approx \pi$ in Fig. 3(b,e) and $\beta \approx \pi/2$ in Fig. 3(c,f)] have also been tested. Again the signal field read out by the probe beam well reproduces the expectation of two petals of equal intensity rotated by an angle $\beta/2$ and bearing a relative π-phase.

In a next step, the case of unbalanced superpositions has been tested (Fig. 4). Such a configuration is experimentally produced by modifying the phase induced by the Berek compensator so as to produce an elliptical polarization before the q-plate [See section 1, Supporting Information]. The associated intensity pattern must then feature two petals superimposed with a residual background contribution since:

$$I = \left| a_1 e^{i\varphi} + a_{-1} e^{i\beta} e^{-i\varphi} \right|^2 = 1 + 2a_1 a_{-1} \cos(2\varphi - \beta). \quad (7)$$

For $a_1 \neq a_{-1}$ and $a_1^2 + a_{-1}^2 = 1$, one has $a_1 a_{-1} < 1/2$. The previous equation therefore indicates that no angle φ cancels the intensity unlike balanced qubit, providing therefore an intensity pattern with two lobes surrounded by a "figure-eight halo". The experiment described below was conducted with a Berek compensator set to produce a superposition with $a_1 = 2\ a_{-1}$. The intensity pattern measured for the input and signal beams (at $\tau = 21.18$ ps) are depicted in Fig. 4(a) and (b). As evident, these last display the anticipated figure-eight halo. In order to compare the input and restored beams, we have extracted their angular distribution in Fig. 4(c). The figure reveals a high degree of similarities between the two distributions which is a strong indicator of the quality of the restoration. The relative contribution

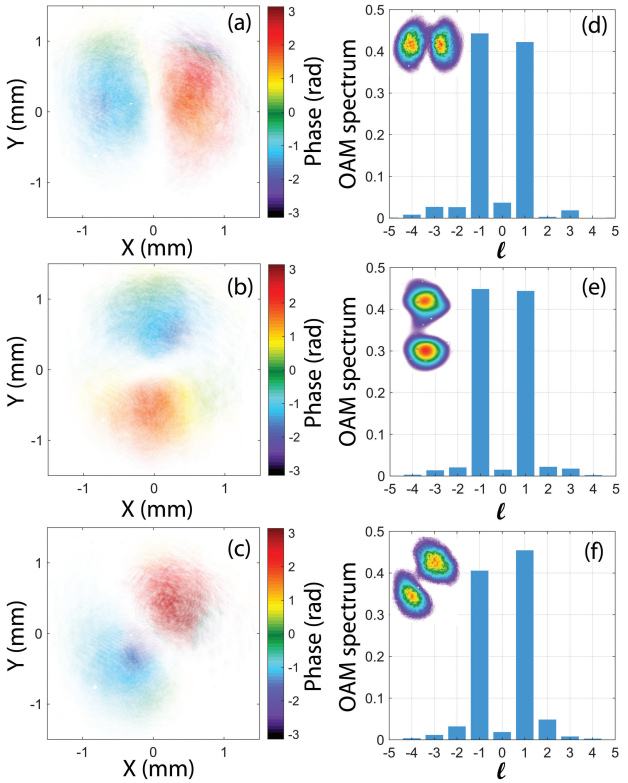

Figure 3 Storage of a balanced superposition $\ell = \pm 1$ with in (a, d) $\beta \approx 0$, (b, e) $\beta \approx \pi$, (c, f) $\beta \approx \pi/2$. Left column: spatial distribution of the restored field with its spatial phase as a color scale. Right column: decomposition of the signal field into first OAM eigenstates, the inset depicts the spatial distribution of the input beam stored in the molecular sample.

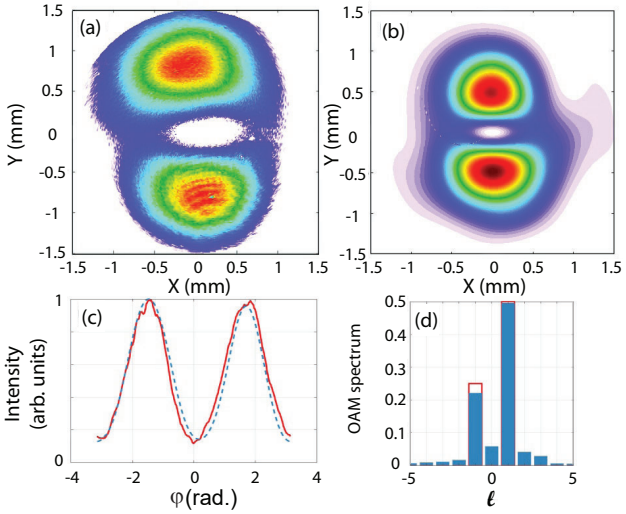

Figure 4 Superposition of unbalanced $\ell = \pm 1$ OAM states. (a) intensity pattern of the input pump beam to be stored, (b) intensity pattern of the measured signal field, (c) dashed blue (resp. solid red) angular distribution of the integrated signals depicted in b (resp. a), (d) decomposition of the signal field into the first OAM eigenstates (blue square) compared to the encoded ratio a_1/a_{-1} (red line) evaluated from the contrast measured in (c).

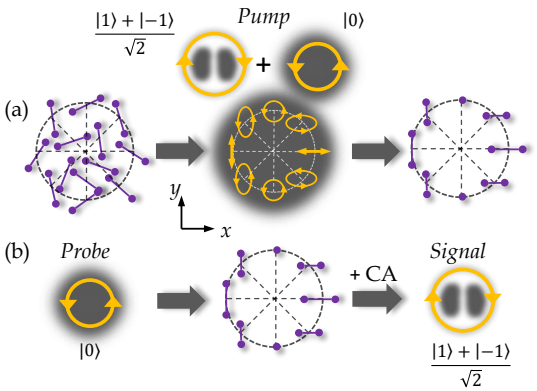

Figure 5 (a) Mechanism for storing $|\Psi\rangle_{\text{in}} = \frac{|1\rangle+|-1\rangle}{\sqrt{2}}$: the superposition of $|\Psi\rangle_{\text{in}}$ with the auxiliary beam ($|0\rangle$) of opposite helicities provides a global field with an azimuthal distribution of amplitude and polarization inducing a spatially varying molecular alignment. A schematic representation of the axis of alignment with its amplitude is depicted on the right part. (b) The interaction of a circularly-polarized probe field with the molecular sample at the occurrence of molecular alignment produces a field of opposite handedness (isolated by a circular analyzer CA) embedding $|\Psi\rangle_{\text{in}}$.

$\ell = \pm 1$ (a_1 and a_{-1}) in the input beam can further be retrieved through the contrast of the angular distribution from Eq. 7. The result, shown as a red line in Fig. 4(d), is found to be in good agreement with the modulation $a_1 = 2\, a_{-1}$ applied in the input beam and with the complete decomposition of the restored beam.

The above results demonstrating the storage of OAM modes superposition into rotational coherences can be interpreted by the field-induced spatial structuring of the molecular sample. A typical example is depicted in Fig. 5 for the case of $|\Psi\rangle_{\text{in}} = (|1\rangle + |-1\rangle)/\sqrt{2}$ ($a_1 = a_{-1}$ with $\beta = 0$). The associated input field can be written as $E_{\text{R}}(t,\varphi) = \varepsilon_0(t)\cos(\varphi)e^{-i\omega_0 t}$ and its superposition with the auxiliary beam of opposite helicities provides a field with an azimuthal distribution of amplitude and ellipticity as depicted in the middle part of Fig. 5(a) [See also section 4, Supporting Information]. The light-matter interaction tends to align the molecules along the axis of the field but with a degree of alignment in the (x,y) plane that decreases as the ellipticity increases. [38] As a result, the molecules are predominantly aligned along the x-axis in the region $-\pi/2 < \varphi < \pi/2$ (right part of the interaction area) but with a degree of alignment which decreases with $|\varphi|$. In particular for $\varphi = \pi/2$, the pump field is perfectly circularly polarized so that the axis of molecular alignment points towards z, the propagation axis. As a function of the time, the molecules will be alternately confined along z or delocalized in the transverse plane without any preferential direction. There is therefore

no net anisotropy in the $x-y$ plane for $\varphi = \pi/2$. The same situation occurs for the left part of the interaction area but with molecules preferentially aligned along the y-axis. This result is confirmed by the Hamiltonian interaction given in Eq. 4. For the input field $E_R(t,\varphi) = \varepsilon_0(t)\cos(\varphi)e^{-i\omega_0 t}$ under consideration, we have $a_s(\varphi) = |\cos(\varphi)|$ and $\phi_s = 0$ (resp. π) in the right (resp. left) part of the interaction area in Fig. 5(a). As already explained, the molecules will be confined along the angle $\Phi = \frac{\phi_s}{2}$ and therefore along the x (resp. y)-axis in the right (resp. left) part of the beam profile with a coupling term that varies as $a_s(\varphi) = |\cos(\varphi)|$. This spatial structuring of the sample leads to an azimuthal variation of its anisotropy in the (x,y) plane, this last being maximal for $\varphi = [0,\pi]$ and zero for $\varphi = \pm\pi/2$. A circularly polarized probe beam interacting with such a sample will experience a spatially-dependent modification of its ellipticity enabling to restore the OAM mode or OAM mode superposition after a circular analyzer. It produces for the case $|\Psi\rangle_{\text{in}} = \frac{|1\rangle+|-1\rangle}{\sqrt{2}}$ a signal with two petals located at $\varphi = 0$ and π that are phase-shifted by π as a result of the orthogonal direction of the molecules in the right and left part of the interaction area [Fig. 5(b)]. From the birefringence of the molecular sample, it can readily be shown [See section 4, Supporting Information] that the signal field is of the form $E_{\text{sig}} \propto \cos(\varphi)$ that corresponds to the photon state $|\Psi\rangle_{\text{in}} = (|1\rangle + |-1\rangle)/\sqrt{2}$ stored in the molecular sample.

5. Conclusion

We have shown the storage of OAM modes superpositions carried by ultrashort laser pulses into rotational coherences of a molecular system. The approach, exploiting the field-free molecular alignment and the interplay between SAM and OAM, features the ability to store both the spatial phase and amplitude of light beams. The storage mechanism can be interpreted by the production of a time-varying spatial pattern of aligned molecules in three dimensions embedding the spatial structure of the beam to be stored. Once produced, this pattern can restore the spatial information into a reading beam. The storage time relying on molecular alignment is of the order of 100 ps in the condition of the present work but can be increased up to several nanoseconds [39] if the gas density is reduced. Furthermore, while the storage time is a crucial parameter for long-distance communication, such a coherent buffer memory can be attractive for ultrafast local quantum processing where other properties as the bandwidth and multi-mode ability can be of more interest. [40] Besides applications as THz-bandwidth storage medium, the strategy exploiting molecules as light-matter interface features interesting prospects for various applications. The present strategy could be for instance applied for the design of q-plates enabling to generate beams with a superposition of various ℓ-values. Standard q-plates, used for embedding pure OAM states, usually rely on liquid crystal films carefully orientated with a specific pattern in the plane perpendicular to the plate surface. A 3D-design, as prescribed in the present work, would allow an extension of the method to impart OAM superpositions. The rich structure of rotational states also constitutes a specific attribute of molecules compared to atoms. This specificity could be exploited to store complex waveform as space-time wavepackets embedding time-varying OAM [41] or multiplexed light embedding both SAM and OAM. [31,32] Finally, the set of strategies developed this last decades to control the rotational coherences and the angular distribution of molecules in space [42–45] could be of great interest for the manipulation and tunability of OAM beams. A controllable laser-induced modification of the molecular pattern and therefore of the state stored by the molecular sample constitutes the basic building block of quantum logic gates and can be exploited to produce complex optical waveforms with a spatially (and possibly time) varying phase and amplitude structure.

Acknowledgments: this work was supported by the Conseil Régional de Bourgogne Franche-Comté, the CNRS, the EIPHI Graduate School (contract"ANR-17-EURE-0002") and has benefited from the facilities of the SMARTLIGHT platform in Bourgogne Franche-Comté (EQUIPEX+ contract "ANR-21-ESRE-0040")

Key words: orbital angular momentum, ultrashort optical vortex, field-free molecular alignment, spatial shaping

References

[1] T. Brixner, G. Gerber, *ChemPhysChem.* **2003**, *4*, 418.
[2] H. Qi, Z. Lian, D. Fei, Z. Chen, Z. Hu, *Adv Phys-X* **2021**, *6*, 1949390.
[3] B. Neuenschwander, B. Jaeggi, M. Schmid, G. Hennig *Physics Procedia* **2014**, *56*, 1047.
[4] A. M. Weiner, *Opt. Commun.* **2011**, *284*, 3669.
[5] J. Kasparian, M. Rodriguez, G. Méjean, J. Yu, E. Salmon, H. Wille, R. Bourayou, S. Frey, Y.-B. André, A. Mysyrowicz, R. Sauerbrey, J.-P. Wolf, L. Wöste, *Science* **2003**, *301*, 61.
[6] G. P. Agrawal, *Optics in Our Time*, Springer International Publishing, **2016**, *8*, 177
[7] A. I. Lvovsky, B. C. Sanders, W. Tittel, *Nat. Photonics* **2009**, *3*, 706.
[8] L. Allen, M. W. Beijersbergen, R. J. C. Spreeuw, J. P. Woerdman, *Phys. Rev. A* **1992**, *45*, 8185.
[9] M. J. Padgett, *Opt. Express* **2017**, *25*, 11265.
[10] Y. Shen, X. Wang, Z. Xie, C. Min, X. Fu, Q. Liu, M. Gong, X. Yuan, *Light Sci. Appl.* **2019**, *8*, 90.
[11] A. Forbes, *Laser Photonics Rev.* **2019**, *1900140*, 1.
[12] R. Inoue, N. Kanai, T. Yonehara, Y. Miyamoto, M. Koashi, M. Kozuma, *Phys. Rev. A* **2006**, *74*, 053809.
[13] D. S. Ding, Z. Y. Zhou, B. S. Shi, G. C. Guo, *Nat. Commun.* **2013**, *4*, 2527.
[14] A. Nicolas, L. Veissier, L. Giner, E. Giacobino, D. Maxein, J. Laurat, *Nat. Photonics* **2014**, *8*, 234.
[15] A. Rubano, F. Cardano, B. Piccirillo, L. Marrucci, *J. Opt. Soc. Am. B* **2019**, *36*, 70.
[16] M. Yessenov, J. Free, Z. Chen, E. G. Johnson, M. P. J. Lavery, M. A. Alonso and A. F. Abouraddy, *Nature Comm.* **2022**, *13*.
[17] H. He, M. E. J. Friese, N. R. Heckenberg, H. Rubinsztein-Dunlop, *Phys. Rev. Lett.* **1995**, *75*, 826.

[18] N. B. Simpson, K. Dholakia, L. Allen, M. J. Padgett, *Opt. Lett.* **1997**, *22*, 52.

[19] A. J. F. de Almeida, S. Barreiro, W. S. Martins, R. A. de Oliveira, D. Felinto, L. Pruvost, J. W. R. Tabosa, *Opt. Lett.* **2015**, *40*, 2545.

[20] A. Sit, F. Bouchard, R. Fickler, J. Gagnon-Bischoff, H. Larocque, K. Heshami, D. Elser, C. Peuntinger, K. Günthner, B. Heim, C. Marquardt, G. Leuchs, R. W. Boyd, E. Karimi, *Optica* **2017**, *4*, 1006.

[21] J. Pinnell, I. Nape, M. de Oliveira, N. Tabebordbar, A. Forbes, *Laser Photon Rev.* **2020**, *14*, 2000012.

[22] Y. Yan, G. Xie, M. P. J. Lavery, H. Huang, N. Ahmed, C. Bao, Y. Ren, Y. Cao, L. Li, Z. Zhao, A. F. Molisch, M. Tur, M. J. Padgett, A. E. Willner, *Nat. Commun.* **2014**, *5*, 4876.

[23] J. Wang, J. Y. Yang, I. M. Fazal, N. Ahmed, Y. Yan, H. Huang, Y. Ren, Y. Yue, S. Dolinar, M. Tur, A. E. Willner, *Nat. Photonics* **2012**, *6*, 488.

[24] P. Béjot, B. Kibler, *ACS Photonics* **2021**, *8*, 2345.

[25] P. Béjot, B. Kibler, *ACS Photonics* **2022**, *9*, 2066.

[26] Q. Zhan, *Adv. Opt. Photon.***2009**, *1*, 1.

[27] F. Tamburini, G. Anzolin, G. Umbriaco, A. Bianchini, C. Barbieri, *Phys. Rev. Lett.* **2006**, *97*, 163903.

[28] K. A. Forbes, D.L. Andrews, *JPhys photonics* **2021**, *3*, 022007.

[29] J. L. Bégin, A. Jain, A. Parks, F. Hufnagel, P. Corkum, E. Karimi, T. Brabec and Ravi Bhardwaj, *Nat. photonics* **2022**, *17*, 82.

[30] M. Fanciull, M. Pancaldi, E. Pedersoli, M. Vimal, D. Bresteau, M. Luttmann, D. De Angelis, P. Rebernik Ribič, B. Rösner, C. David, C. Spezzani, M. Manfredda, R. Sousa, I-L. Prejbeanu, L. Vila, B. Dieny, G. De Ninno, F. Capotondi, M. Sacchi and T. Ruchon, *Phys. Rev. Lett.* **2022**, *128*, 077401.

[31] K. E. Ballantine, J. F. Donegan and P. R. Eastham, *Sci. Adv.* **2016**, *2*, e1501748.

[32] M. Luttmann, M. Vimal, M. Guer, J-F Hergott, A. Z. Khoury, C. Hernández-García, E. Pisanty and T. Ruchon, *Sci. Adv.* **2023**, *9*, 3486.

[33] F. Trawi, F. Billard, O. Faucher, P. Béjot, E. Hertz, *Laser Photonics Rev.* **2023**, *17*, 2200525.

[34] V. Renard, M. Renard, S. Guérin, Y. T. Pashayan, B. Lavorel, O. Faucher, H. R. Jauslin, *Phys. Rev. Lett.* **2003**, *90*, 153601.

[35] K. Y. Bliokh, E. A. Ostrovskaya, M. A. Alonso, O. G. Rodriguez-Herrera, D. Lara, C. Dainty, *Opt. Express* **2011**, *27*, 26132.

[36] C. T. Schmiegelow, J. Schulz, H. Kaufmann, T. Ruster, U. G. Poschinger, F. Schmidt-Kaler, *Nat. Commun.* **2016**, *7*, 12998.

[37] A. Rouzée, V. Renard, S. Guérin, O. Faucher, and B. Lavorel, *Phys. Rev. A* **2007**, *75*, 013419.

[38] E. Hertz, D. Daems, S. Guérin, H. R. Jauslin, B. Lavorel, O. Faucher, *Phys. Rev. A* **2007**, *76*, 043423.

[39] A. A. Milner, A. Korobenko, V. Milner, *Phys. Rev. A* **2016**, *93*, 053408.

[40] K. Heshami, D. G. England, P. C. Humphreys, P. J. Bustard, V. M. Acosta, J. Nunn, B. J. Sussman, *J. Mod. Opt.* **2016**, *63*, 2005.

[41] D. Cruz-Delgado, S. Yerolatsitis, N. K. Fontaine, D. N. Christodoulides, R. Amezcua-Correa, M. A. Bandres, *Nat. Photonics* **2022**, 1-6.

[42] E. Hertz, A. Rouzée, S. Guérin, B. Lavorel, O. Faucher, Phys. Rev. A **75**(3), 031403 (2007).

[43] A. Rouzée, E. Hertz, B. Lavorel, O. Faucher, *J. Phys. B* **2008**, *41*, 074002.

[44] O. Korech, U. Steinitz, R. Gordon, I. Sh. Averbukh, Y. Prior, *Nat. Photonics* **2013**, *7*, 711.

[45] G. Karras, M. Ndong, E. Hertz, D. Sugny, F. Billard, B. Lavorel, O. Faucher, *Phys. Rev. Lett.* **2015**, *114*, 103001.